HKIE THE HONG KONG INSTITUTION OF ENGINEERS 香港工程師學會

Numerical study of electrochemical thermocells for harvesting low-grade waste heat

Chun Cheng[1,*], Shien-Ping Feng[2] and Meng Ni[1]

[1] Department of Building and Real Estate, Research Institute for Sustainable Urban Development (RISUD) & Research Institute for Smart Energy (RISE), The Hong Kong Polytechnic University, Hong Kong, People's Republic of China

[2] Department of Advanced Design and System Engineering (ADSE), City University of Hong Kong, Hong Kong, People's Republic of China

ABSTRACT

Experimental studies on electrochemical thermocells or thermogalvanic cells have demonstrated their potential for low-grade heat utilisation, but the numerical studies on these systems are lacking. In this study, a mathematical model is developed to simulate the transport and electrochemical processes in the thermocells. After model validation, parametric simulations are conducted to understand the effects of various operational and structural parameters on thermocell performance. The studied parameters include the concentration of redox couples, temperature difference between anode and cathode, size of thermocell and the thickness and location of the separator. It is found that a higher concentration of redox couples and larger temperature difference between the two electrodes benefit thermocell performance. It is also interesting to find that vertically arranged thermocells produce a higher power density than that of horizontally arranged thermocells by 13.85%. Besides, the power density is increased by approximately 30% if the separator is attached to the cathode in comparison to the non-separator condition. Optimal values of the structural parameters are identified. This research clearly demonstrates that the performance improvement of thermocells depends on not only electrochemistry and materials, but also engineering design optimisation.

KEYWORDS Thermocells; thermogalvanic cell; harvesting low-grade waste heat; modelling; simulation

CONTACT Chun Cheng 19044312r@connect.polyu.hk

Received 27 January 2022

1. Introduction

A considerable amount of waste heat from industrial facilities and solar radiation is discarded into the environment without efficient utilisation every year. A large proportion of this waste heat is low-grade waste heat below 150°C (Cheng et al., 2020). This causes not only energy waste, but also environmentally-unfriendly thermal pollution. Although efforts have been made to develop technologies for heat-to-electricity conversion in the last few decades, the energy conversion efficiency is still very low due to the Carnot efficiency limitation. Generally, two main mature approaches including indirect and direct methods have been developed for low-grade waste heat harvesting. In the indirect methods, the waste heat is converted into mechanical energy or other forms of energy first, and is subsequently transformed into electrical energy. A typical case is the Organic Rankine Cycle (ORC) (Rahbar et al., 2017). In the direct methods, typical thermoelectric (TE) devices mainly rely on the heat-induced electrons from the semiconductor material when the two ends of the materials are under two different temperatures. Additionally, electrochemical thermocells appear to be more promising due to their low cost in comparison to TE devices.

Electrochemical thermocells are based on the temperature-induced voltage difference of the two electrodes for power generation. As shown in Figure 1, a thermocell is composed of two electrodes, separated by an electrolyte with redox couples of a certain concentration. Under a temperature difference applied between the two electrodes, a voltage is established due to the temperature response from the redox couples. As the oxidation reaction and the reduction reaction are reverse reactions, they share common reactants and products. When the oxidation and reduction reactions simultaneously occur at the two electrodes, current is theoretically generated without any change in the total amount of the substances. Therefore, if there is no degradation of the redox couples, a sustainable and stable current and voltage can be delivered under certain working conditions with heat as the input energy. During the electricity generation process, a complete system involves highly coupled heat transfer, mass transfer and electrode electrochemical reaction processes.

A large amount of thermocell-based experimental research has been reported in the past few years, most of which has focused on the exploration of suitable redox couples and optimisation of electrodes and electrolytes. Initially, aqueous redox couples such as aqueous ferricyanide/ferrocyanide and iron/ferrous ions were employed in the thermocells with a low power density (< 10 W m^{-2}) (Rahimi et al., 2018). Thus, a series of methods for enhancing the temperature response of redox couples to widen the operation voltage window and furthermore increase the power output have been proposed and evaluated. The most widely reported approaches include adding additives and changing the aqueous electrolyte into an organic electrolyte. Although these approaches can enhance the heat-generated voltage,

*The first author who was at the age of 35 or below on the closing date of submission to the HKIE Outstanding Paper Award for Young Engineers / Researchers 2022.

the power density of the thermocell cannot be improved significantly and can even be decreased in some cases (Al-Masri et al., 2018; Duan et al., 2018; Kim et al., 2019; Taheri et al., 2019). This is mainly due to the higher ohmic loss caused by additives or the organic environment in comparison to conventional aqueous electrolytes. Besides, a lot of works have been done to optimise the electrodes and cell configuration. The highest power density record (12 W m^{-2}) was achieved in Long Zhang's work by changing the electrode from platinum to being carbon-based, increasing the concentration of the redox couple and optimising the separator (Zhang et al., 2017). Despite the many experimental works, no comprehensive theoretical or numerical study has been conducted on thermocells to understand the effects of various structural and operational parameters on thermocell performance, which would be useful for subsequent design optimisation.

Only a few studies reported mass and heat transfer in thermocells in the last century, namely Sokirko (1994), Ikeshoji et al. (1991) and Kimura (1991). They evaluated the convection effect on the performance of thermocells. As the thermal boundary layers are thicker than the fluid flow boundary layers, the cell orientation of vertical electrodes is preferred to accelerate the mass transfer process. The only recent and complete simulation work on thermocells was conducted by Salazar et al. (2014). It presented the optimisation of cell dimensions and discussed the performance of different cell designs such as stacking cells and flow cells. However, these works did not attempt to systematically evaluate the performance from the perspective of the electrochemical reaction itself. These works simulated the fluid flow and heat transfer inside the thermocells, but explanations for how the internal parameters affect each other and relate to power density are still lacking. With the current thermocell system becoming more and more complex and numerical analysis methods gradually improving, a comprehensive numerical model is urgently needed to guide the optimisation of thermocells.

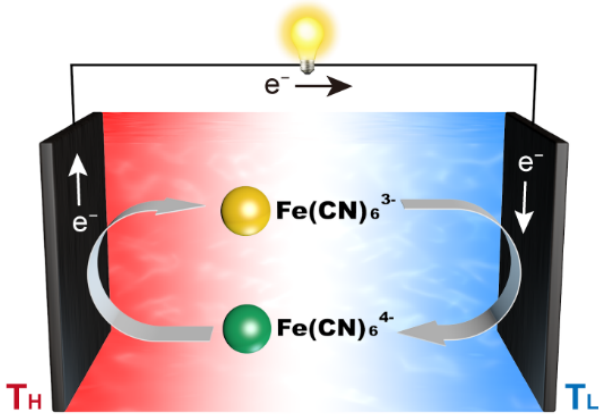

Figure 1. Schematic diagram of a thermocell.

This paper aims to develop a comprehensive mathematical model for thermocells to guide its design optimisation. By coupling the governing equations of heat, mass and charge transfer to describe the thermocell system, this paper studies the effects of concentration of redox couple, temperature difference of the two electrodes, the size of the thermocell and the locations of the separator on the performance of thermocells. Based on parametric simulations, optimal structural and operational parameters are identified for performance improvement.

2. Methods

Figure 1 shows the working principle of an electrochemical thermocell. The electrolyte with redox couple is sandwiched between two electrodes. The products of each electrode travel through the electrolyte and reach the other side to participate in the electrochemical reactions as reactants. As the reactions take place continuously, electrons are produced at the anode and are subsequently transported to the cathode through the external circuit to produce useful power. The following assumptions are adopted in the 2D non-isothermal model: (1) The electrolyte solution is infinitely dilute; thus, the activity values equal to concentrations and ion-ion interactions are neglected (Kielland, 1937); (2) The fluid flow is a laminar flow (Ikeshoji et al., 1991); (3) The temperature coefficient of redox couple is regarded as a constant (Ikeshoji et al., 1991); (4) There is a steady state operation (Sokirko, 1994). The input parameters are given in Table 1. For model validation, the input parameters are adjusted to be consistent with the experimental values. For example, the distance between the cathode and anode is 2.6 mm (Zhang et al., 2017). The temperature-dependent physical parameters such as density and electrolyte conductivity are measured or fitted from the experimental data.

2.1. Governing equations

2.1.1. Electrochemistry

A typical reaction of thermocells is based on the redox couple of $FE(CN)_6^{4-}$ / $FE(CN)_6^{3-}$ and the reaction is $[FE(CN)_6]^{4-} \rightleftharpoons [FE(CN)_6]^{3-} + [e^-]$. When a thermocell with the redox couple $FE(CN)_6^{4-}$ / $FE(CN)_6^{3-}$ is applied with different temperatures on the two electrodes, the forward reaction and the reverse reaction take place at the two electrodes respectively. The reaction is driven by the energy difference between the two sides at different temperatures. The electrode potential E based on the Nernst equation can be obtained as:

$$E = E^\circ + (T - T^\circ)\frac{\Delta S^\circ}{nF} - \frac{RT}{nF}\ln\frac{C_R}{C_O}, \quad (1)$$

Table 1. Parameters used in the simulation.

Parameters [units]	Value
Cell length [mm] (Zhang et al., 2017)	2.6
Electrolyte heat capacity [J kg^{-1} K^{-1}] (Kimura, 1991)	4187
Initial $Fe(CN)_6^{3-}$ concentration [M] (Zhang et al., 2017)	0.9
Initial $Fe(CN)_6^{4-}$ concentration [M] (Zhang et al., 2017)	0.9
Electrolyte density of 0.9 M $Fe(CN)_6^{3-}$/ $Fe(CN)_6^{4-}$ solution[kg m^{-3}]*a	$1207.2+0.2398T-0.0009T^2$
Diffusion coefficient [m^2 s^{-1}] (Sarac, 1993)	$(62.66-0.5336\ T+1.1482\times0.001\ T^2)\times10^{-10}$
Rate constant activation energy [kJ mol^{-1}] (Daum & Enke, 1969)	14.644
Charge transfer coefficient (Spiro, 1964a)	0.5
Standard rate constant [m s^{-1}] (Spiro, 1964b)	6e-6
Electrolyte thermal conductivity [W m^{-1} K^{-1}] (Kimura, 1991)	0.6
Anode temperature [K]	354
Cathode temperature [K]	290
Electrolyte conductivity of 0.9 M $Fe(CN)_6^{3-}$/ $Fe(CN)_6^{4-}$ solution [S m^{-1}] (Zhang et al., 2017)	$0.3008(T-273.15)+13.355$
Electrolyte conductivity of $Fe(CN)_6^{3-}$/ $Fe(CN)_6^{4-}$ solution [S m^{-1}] (Zhang et al., 2017)	$-13.945C^{*2}+32.386C^{*}+0.556$
Kinematic viscosity [cm^2 s]*b (Sarac 1993)	$\exp(-4.818-1808T^{-1}+5.616e5T^{-2})$
Thermal-to-voltage conversion [mV K^{-1}] (Hu, Xu and Luo, 2020)	-1.42
Thermal conductivity of electrolyte with separator [W m^{-1} K^{-1}] (Zhang et al., 2017)	0.43
Conductivity of 0.9 M $Fe(CN)_6^{3-}$/ $Fe(CN)_6^{4-}$ solution in separator [S m^{-1}] (Zhang et al., 2017)	$0.1952(T-273.15)+9.7182$
Permeability [m^{-2}]*c (Qin, Zhang and Mei, 2018)	1e-6
Porosity (Cui et al., 2020)	0.9326

With a lack of reported data, the temperature-dependent diffusion coefficient was at 0.2 M. *a The density was fitted by measuring the solution weight with 100 mL volume under different temperatures. *b According to the experimental results, as the concentration changes, the influence of concentration is minor so that the concentration effect is neglected in this model. *c The permeability was measured based on the referenced method.

where T, ΔS, n, F represent the temperature, entropy change, a number of electrons transferred in the reaction, and Faraday constant respectively. The subscript o suggests the standard state. The term C_R is the reduced species concentration and C_O is the oxidised species concentration. The term $\frac{C_R}{C_O}$ represents the effect of concentration at the electrode surface on the electrode potential. As the Nernst equation is based on the isothermal-isobaric assumption, the $(T-T^\circ)\frac{\Delta S^\circ}{nF}$ displays the electrode potential deviation by temperature change-induced energy change. Therefore, a theoretical open circuit potential V_{oc} is:

$$V_{oc}=E_c-E_a=-\frac{\Delta S^\circ(T_a-T_c)}{nF}+\frac{R}{nF}\left(T_a\ln\frac{C_{R_a}}{C_{O_a}}-T_c\ln\frac{C_{R_c}}{C_{O_c}}\right), \quad (2)$$

where the subscripts a and c represent anode and cathode respectively. To characterise the electrode kinetics, the electrode transfer rate constant k at temperature T can be determined by the given standard rate constant k° at T° and rate constant activation energy G_{act}:

$$k=k^\circ\exp\left[\frac{G_{act}}{R}\left(\frac{1}{T^\circ}-\frac{1}{T}\right)\right]. \quad (3)$$

Therefore, the exchange current density j_0 at temperature T can be described as:

$$j_0 = nFk^{\circ}C^{*}\exp\left[\frac{G_{act}}{R}\left(\frac{1}{T^{\circ}}-\frac{1}{T}\right)\right], \quad (4)$$

where C^* is the initial concentration of the reduced and oxidised species. The initial concentrations of reduced and oxidised species (C_{O}^* and C_{R}^*) are the same ($C^* = C_{\mathrm{O}}^* = C_{\mathrm{R}}^*$). With the exchange current density j_0, the Butler-Volmer equation is applied to describe the relations of net current density and electrochemical overpotential. At the anode and cathode, they are expressed as $j_{\mathrm{a}} = j_0\left[\frac{C_{\mathrm{O}}^{\mathrm{a}}}{C_{\mathrm{O}}^*}\exp\left(\frac{-nF(1-\alpha)\theta_{\mathrm{a}}}{RT_{\mathrm{a}}}\right)-\frac{C_{\mathrm{R}}^{\mathrm{a}}}{C_{\mathrm{R}}^*}\exp\left(\frac{nF\alpha\theta_{\mathrm{a}}}{RT_{\mathrm{a}}}\right)\right]$ and $j_{\mathrm{c}} = j_0\left[\frac{C_{\mathrm{O}}^{\mathrm{c}}}{C_{\mathrm{O}}^*}\exp\left(\frac{-nF(1-\alpha)\theta_{\mathrm{c}}}{RT_{\mathrm{c}}}\right)-\frac{C_{\mathrm{R}}^{\mathrm{c}}}{C_{\mathrm{R}}^*}\exp\left(\frac{nF\alpha\theta_{\mathrm{c}}}{RT_{\mathrm{c}}}\right)\right]$, where α is the charge transfer coefficient and the electrochemical overpotentials at the anode and cathode are θ_{a} and θ_{c} ($\theta_{\mathrm{a}} = E_{\mathrm{a}} - E_{\mathrm{a}}^{\mathrm{eq}}\ \theta_{\mathrm{c}}$, $\theta_{\mathrm{c}} = E_{\mathrm{c}} - E_{\mathrm{c}}^{\mathrm{eq}}$) respectively.

The $E_{\mathrm{a}}^{\mathrm{eq}}$ and $E_{\mathrm{c}}^{\mathrm{eq}}$ are the anode and cathode equilibrium potential respectively. Consequently, by considering the ohmic loss $\Delta\phi^{\omega}$, the working voltage V_{cell} of the thermocell is:

$$V_{\mathrm{cell}} = V_{\mathrm{oc}} - \theta_{\mathrm{a}} - \theta_{\mathrm{c}} - \Delta\phi^{\omega}. \quad (5)$$

2.1.2. Flow field and mass transport

To maintain constant power output, the transport of the oxidised and reduced species also needs to reach a steady state. The resultant ion flux should consider the impact of diffusion, migration, thermal diffusion and convection:

$$\vec{N}_{\mathrm{i}} = -D_{\mathrm{i}}\nabla C_{\mathrm{i}} - Z_{\mathrm{i}}u_{\mathrm{i}}FC_{\mathrm{i}}\nabla\phi - \frac{Q_{\mathrm{i}}}{RT^2}D_{\mathrm{i}}C_{\mathrm{i}}\nabla T + C_{\mathrm{i}}\vec{u}, \quad (6)$$

where $\vec{N}_{\mathrm{i}}$ is the ion flux density, which is composed of oxidised flux density, reduced flux density and counter-ion flux density, D_{i}, C_{i}, Z_{i}, u_{i} and Q_{i} are the diffusion coefficient, concentration, number of charges, ion mobility and heat of ion transport of a certain ion species, ϕ is the electrostatic potential and $\vec{u}$ is the bulk vector velocity. The terms $-D_{\mathrm{i}}\nabla C_{\mathrm{i}}$, $-Z_{\mathrm{i}}u_{\mathrm{i}}FC_{\mathrm{i}}\nabla\phi$, $-\frac{Q_{\mathrm{i}}}{RT^2}D_{\mathrm{i}}C_{\mathrm{i}}\nabla T$ and $C_{\mathrm{i}}\vec{u}$ represent the effects due to diffusion, migration, thermal diffusion and convection respectively.

Particularly, the ion flux of thermal diffusion is driven by the temperature gradient from the hot side to the cold side. The mobility of ions can be expressed by the Nernst-Einstein relationship ($u_{\mathrm{i}} = \frac{D_{\mathrm{i}}FZ_{\mathrm{i}}}{RT}$). The electrical neutrality condition should be satisfied as $\sum Z_{\mathrm{i}}C_{\mathrm{i}} = 0$. In an electrochemical system, the electrical neutrality condition at the electrode is $\vec{N}_{\mathrm{O}}\cdot\vec{n} = -\vec{N}_{\mathrm{R}}\cdot\vec{n}$, where $\vec{N}_{\mathrm{O}}$ and $\vec{N}_{\mathrm{R}}$ are the ion flux density of oxidised and reduced species and $\vec{n}$ is a normal unit vector perpendicular to the electrode. Considering the definition of current density ($\vec{j} = F\sum_i Z_{\mathrm{i}}\vec{N}_{\mathrm{i}}$), the current density perpendicular to the electrode is given as:

$$j = F\sum_i\left(-Z_{\mathrm{i}}D_{\mathrm{i}}\nabla C_{\mathrm{i}} - Z_i^2u_{\mathrm{i}}FC_{\mathrm{i}}\nabla\phi - \frac{Z_{\mathrm{i}}Q_{\mathrm{i}}}{RT^2}D_{\mathrm{i}}C_{\mathrm{i}}\nabla T\right)\cdot \vec{n} + F\sum_i Z_{\mathrm{i}}C_{\mathrm{i}}\vec{u}\cdot\vec{n}. \quad (7)$$

If the system reaches a steady state, the divergence of ion flux density equals zero ($\nabla\cdot\vec{N}_{\mathrm{i}} = 0$).

Navier–Stokes equations are introduced to describe the fluid flow in thermocells. Firstly, considering the density changes with temperature in thermocells, the density can be depicted as a polynomial function of temperature ($\rho = \beta_1 + \beta_2T + \beta_3T^2$). Taking gravitational forces and viscous force into consideration, in a steady state ($\nabla\cdot(\rho\vec{u}) = 0$), the Navier–Stokes equation is presented as below (Salazar et al., 2014):

$$(\vec{u}\cdot\nabla)\vec{u} = v\nabla^2\vec{u} + \vec{g}\left(\frac{\rho_{\mathrm{o}}-\rho}{\rho_{\mathrm{o}}}\right), \quad (8)$$

where v is the kinematic viscosity. If a separator is added between the cathode and the anode, for the mass transfer of the incompressible fluid in the porous medium, since the velocity divergence is equal to 0, the equation can be written as follows:

$$\rho(\vec{u}\cdot\nabla\vec{u}) = -\nabla p + \nabla\cdot\left(\mu(\nabla\vec{u} + (\nabla\vec{u})^T)\right) - \frac{\varepsilon v\vec{u}}{K} + \rho\vec{g}\left(\frac{\rho_{\mathrm{o}}-\rho}{\rho_{\mathrm{o}}}\right), \quad (9)$$

where p is the pressure, ε is the porosity of the porous separator, μ is the dynamic viscosity and K is the coefficient of permeability. The last term on the right-hand side of the equation is the Darcy's term to describe the momentum transport of liquid in a porous separator. This term is cancelled for momentum transport in bulk electrolyte. It should be noted that the effective diffusion coefficient in the porous medium is different from the first term on the right-hand side of Equation (9). The effective coefficient needs to be pre-defined by tortuosity and porosity to simulate the diffusion process in the porous medium.

2.1.3. Heat transfer

Constant temperatures of the two electrodes are specified as the boundary conditions in this model. The temperature range is limited to the boiling point of water to avoid additional heat being required for a phase change. The heat transfer in the electrolyte is governed by:

$$\rho C_{\mathrm{p}}\vec{u}\cdot\nabla T = \nabla\cdot(\kappa_{\mathrm{s}}\nabla T + \sum D_{\mathrm{i}}Q_{\mathrm{i}}\nabla C_{\mathrm{i}}) + S, \quad (10)$$

where C_{p} is the heat capacity, κ_{s} is the electrolyte thermal conductivity and S is the heat generation sources including the irreversible heat from activation overpotential and

Joule heat. It was proved that the irreversible heat is three orders of magnitude lower than conductive-convective heat transfer (Quickenden and Mua, 1995); thus, it can be neglected in this model. However, the heat generation term cannot be neglected if the current density is further extended in the future while the conductive-convection heat transfer is not significant under some operating conditions.

2.1.4. Efficiency

The efficiency η is the ratio of maximum power density to heat flux density. As the maximum power is the working voltage V_{cell} multiplied by current density j, the absolute efficiency is given as $\eta[\%] = \frac{V_{cell} \cdot j}{q}(100)$. Due to the Carnot limitation, the relative efficiency η_r is expressed as the ratio of absolute efficiency to the Carnot efficiency η_c. It is written as $\eta_c = \frac{\Delta T}{T_H}$ and $\eta_r = \frac{\eta}{\eta_c}$, where ΔT is the temperature difference of two electrodes and T_H is the value of the high temperature.

3. Results and discussion

3.1. Model validation

The governing equations were solved by using the finite element method. The model was developed in COMSOL 5.6 and solved by a Multifrontal Massively Parallel sparse direct solver (MUMPS). Preliminary simulation was conducted for comparison with the experimental data from the literature. In the experiment, the thermocell works with the temperature difference of 86 K in the electrolyte of 0.9 M redox couple, with a 2-mm separator sandwiched between the two electrodes at a distance of 2.6 mm. The electrode is a platinum foil in the shape of a square with a side length of 1 cm. To reduce the cost, Pt could be electrodeposited on the surface of base metal substrates while ensuring good conductivity. The operating parameters are shown in Table 1. In all simulations, all boundaries were meshed with a very small size of 3.9×10^{-7} m. Figure 2(a) shows the results of grid independence analysis. It can be seen that the peak power density reaches a constant value when the number of degrees of freedom is higher than 53,907 with solution time of 38 minutes. To ensure grid-independence of the simulation results, the degrees of freedom of 87,815 with meshing elements of 12,288 were adopted in this study. The good agreement between the simulation results and experimental data (from supplementary information of reference (Zhang et al., 2017) shown in Figure 2(b)) validates the model well for subsequent parametric simulation and design optimisation.

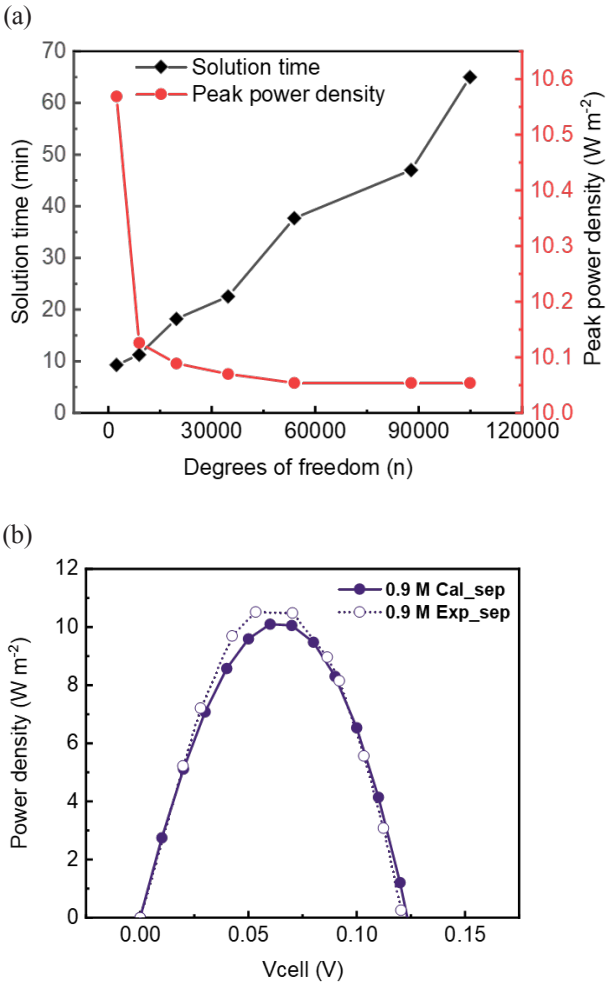

Figure 2. Model validation. (a) Grid independence analysis; and (b) Data validation. The cell is designed with a 2-mm separator. The calculated result and experimental result are plotted in this figure.

3.2. Working performance

By coupling the governing equations, a comprehensive model was developed to describe the thermocell system. Conventional thermocells apply $K_3Fe(CN)_6/K_4Fe(CN)_6$ as redox couple. The concentration of $Fe(CN)_6^{3-}$ /$Fe(CN)_6^{4-}$ should be restricted to 0.4 M due to their solubility limitation. However, it can be significantly improved to 0.9 M by switching to cations (Zhang et al., 2017). To be consistent with the working conditions in the literature (Zhang et al., 2017), the internal temperature difference and the concentration were set to be 64 K and 0.9 M respectively. The thermocell was designed as a square with a side length of 2.6 mm. A Pt electrode was applied. As shown in Figure 3(a), the peak power density appears at approximately half of the OCV. Figure 3(b) shows the temperature distribution in the electrolyte. According to the electrode kinetics, the temperature-dependent rate constant at the low-temperature electrode is lower than

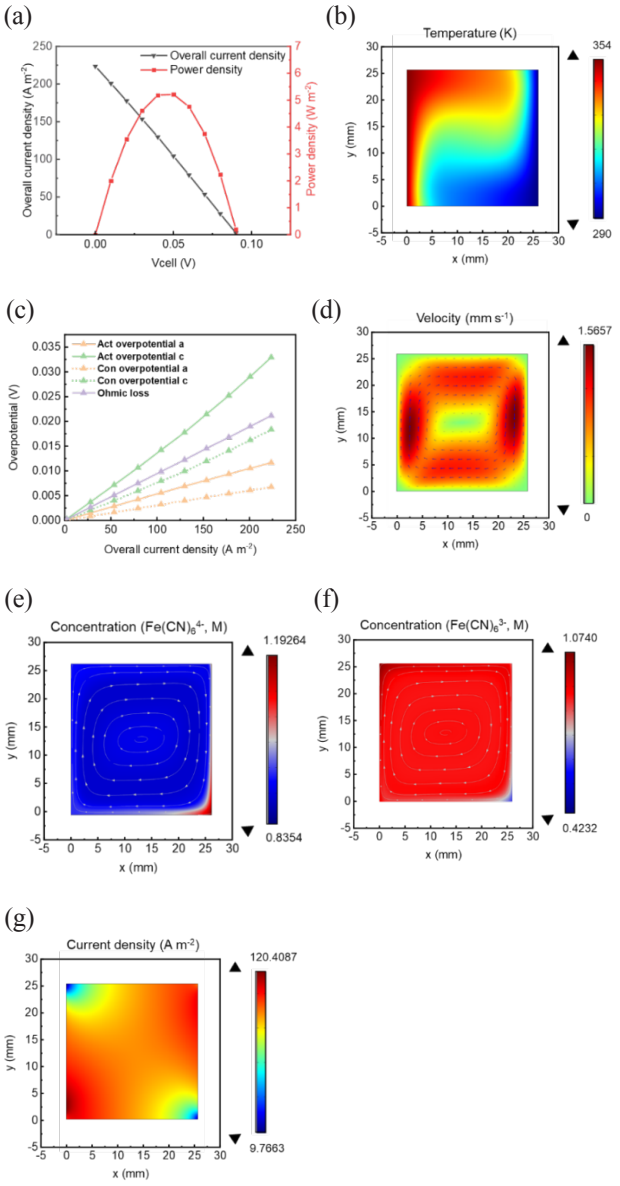

Figure 3. Performance of a traditional thermocell. (a) The performance of power density and current density in a 0.9 M $Fe(CN)_6^{3-}$ /$Fe(CN)_6^{4-}$ system with a temperature difference of 64 K; (b) temperature (K) distribution in the thermocell; (c) the overpotentials including ohmic loss, activation overpotentials and concentration overpotential of the anode and cathode corresponding to the working condition in Figure 3(a); (d) velocity (mm s^{-1}); (e) distribution of $Fe(CN)_6^{4-}$ and (f) $Fe(CN)_6^{3-}$ when the thermocell reaches a steady state; and (g) distribution of current density in line with the working condition of peak power in Figure 3(a).

that at the high-temperature electrode. Thus, the theoretical exchange current density at the low-temperature electrode is lower than that at the high-temperature electrode. As a consequence, the peak current density approaches the limiting current density of the cathode before that of the anode, and the resultant activation overpotential of the cathode overwhelms that of the anode under the same current density. Despite the reaction rate difference, the ion diffusion process is also restricted by the relatively low diffusion coefficient (3.2709×10^{-10} m^2 s^{-1} at the cathode and 2.1479×10^{-9} m^2 s^{-1} at the anode) of ions from the cathode to the anode. In other words, the products generated at the cathode are less likely to diffuse and are easily restricted by mass transfer. To sum up, the power density is restricted by the cold electrode.

Since the concentration overpotential is defined as the concentration discrepancy effect on the potential, the term $\frac{R}{nF}(T_a \ln\frac{C_{R_a}}{C_{O_a}} - T_c \ln\frac{C_{R_c}}{C_{O_c}})$ is determined to be the concentration overpotential in Figure 3(c). As the electrochemical reactions (cause of current density) rely on the local concentration of reactants and products as depicted in equations related to j_a and j_c, the activation overpotential deviates from the normal exponential trend. It can be seen from Figure 3(c) that the activation overpotential of the cathode dominates the total overpotentials as expected. Figure 3(d) shows the flow in a clockwise direction inside the cell under the influence of gravity. It is easy to understand that the fluid flow is driven by natural convection due to the lower density of the electrolyte at the high-temperature end. Natural convection helps to accelerate the mass transfer and heat transfer and eliminates the concentration overpotential caused by the accumulation of products on the electrode surface. Figures 3(e) and 3(f) profiles the ion distribution in the electrolyte. Since the flow velocity of the electrolyte at the corners is almost zero, the product gathers in the corner of the battery in the direction of the electrolyte flow and further affects the local potential and current density (Figure 3(g)).

3.3. Effect of concentration

According to the experimental results (Zhang et al., 2017), the thermal conductivity hardly changes with the concentration but the conductivity of the solution rises sharply as the concentration increases. Therefore, the conductivity coefficient was firstly adjusted according to the concentration of the electrolyte based on the experimental results as shown in Table 1. The effect of concentration on the performance of thermocells, as shown in Figure 4, was then studied. The internal temperature difference is 64 K and the thermocell is designed as a square with a side length of 2.6 mm. Figure 4(a) shows the power density as a function of the concentration and working voltage. The maximum mean power density is improved significantly by increasing the concentration of redox couple due to the

greatly improved current density. It is reasonable to predict the ascendant current density with increased concentration based on the concentration-dependent kinetics, which agree with the multiplied growth in power density in Figure 4(a). Assuming that the thermal conductivity and heat capacity are independent of the electrolyte concentration, the resultant input heat flux densities at different concentrations are almost the same. Thus, the relative efficiency increases nearly seven times from 0.8102% at 0.1 M to 6.3806% at 0.9 M. At the same time, the high concentration results in a greater exchange current density, which decreases the activation overpotential under the same working current density. This effect can be seen in Figure 4(c). Since all the maximum power densities occur when the working potential is half of the open circuit voltage, all thermocells operating under different concentrations of electrolyte have the same overpotential at maximum power density, and the activation overpotential proportion increases as expected. With regard to the concentration overpotential, the concentration fluctuation caused by the reaction has a minor effect on the high-concentration electrolyte, which helps to stabilise the ratio of oxidised species to reduced species, which further decreases the concentration overpotential. However, the higher current density results in a higher ohmic loss as the concentration-induced increment in conductivity does not balance the influence from the current density as depicted in Figure 4(c). The model and parameters were tested out with experimental data (Zhang et al., 2017). Under the same working condition, the calculated power density fairly matches the trend of the reported experimental value. The measured peak power density is higher than the calculated value. This is because the effect of temperature on electrolyte conductivity is not considered in the model, which demonstrates the importance of temperature effect on electrolyte conductivity. To improve the accuracy of simulation, the temperature effect on conductivity was considered and additional simulation was conducted. The updated modelling results agree very well with the experimental values as shown in Figure 4(d).

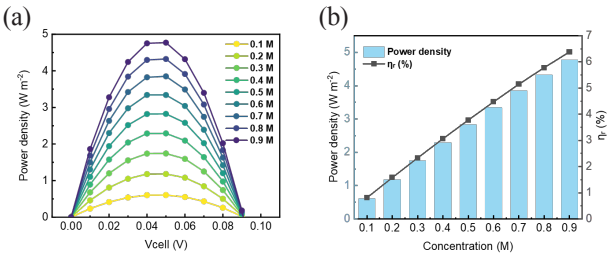

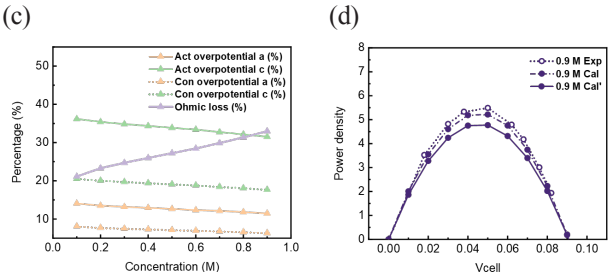

Figure 4. Effect of concentration. (a) The performances of power density versus increasing working voltage at different concentrations of redox couple (ΔT = 64 K); (b) the peak power densities and relative efficiencies performed in electrolytes with different concentrations of redox couple; (c) the proportions of various overpotentials to total overpotential; and (d) the data validation: the line marked in Cal' is the calculated data when the conductivity is only a function of concentration and does not change with temperature; the line marked in Cal is the calculated data after calibration of temperature to conductivity.

3.4. Effect of temperature difference

To study the effect of temperature difference, the concentration of electrolyte and the size of the thermocell are fixed as 0.9 M and 2.6 mm respectively. Since the OCV results from the temperature coefficient and the temperature difference between two electrodes, there is an evident increase in OCV as the temperature difference increases by considering the temperature coefficient as a constant value (Figure 5(a)). A large temperature difference can not only create a large OCV to increase the power density but also increase the Carnot efficiency and the relative efficiency as presented in Figure 5(b). However, the limitation of the cathode becomes more prominent when the temperature difference becomes larger. Since the exchange current density of a thermocell is a function of temperature, it is found that the exchange current density on the high-temperature side is much greater than that on the low-temperature side. As the temperature rises and the current density continues to increase, this ratio of current density to exchange current density will become higher and makes the activation overpotential of the cathode larger (Figure 5(c)). According to the ratio of reactants and products at the cathode (low temperature) and anode (high temperature) respectively, the degree of the concentration overpotential can be estimated. In Figure 5(d), it is shown that this ratio change for the cathode is greater than that for the anode as the temperature increases. In the region where the temperature difference increases from 10 K to 90 K, the reactant to product ratio at the anode has been stabilised above 0.9, but this ratio at the cathode continues to decrease as the temperature difference increases. The temperature change is based on the assumption that the temperature at the low-temperature side does not change while the temperature at the high-temperature end is

adjusted. In addition, the ion diffusion coefficient increases with the increase of temperature. Therefore, compared with a cathode at a lower temperature, the ion diffusion of the anode is relatively easy, so the concentration overpotential is lower. It can be seen that the cathode kinetics limits the performance of thermocells for a larger temperature difference based on the above analysis. However, the ohmic loss does not have a significant impact on the power density at higher current densities as the ohmic loss does not change much under the condition of high current density. This is because the conductivity of the electrolyte at high temperatures is increased significantly. For example, the conductivity of 0.9 M redox couple at 370 K is almost seven times that at 280 K, so the ohmic loss does not change much at high current densities (Figure 5(e)). Although the larger temperature difference results in a higher peak power density, little attention has been paid to breaking the temperature limit in aqueous electrolyte. A possible solution is adding additives or exploiting hybrid electrolytes to adjust the boiling point. This helps to enlarge the operation temperature window and increase the power density.

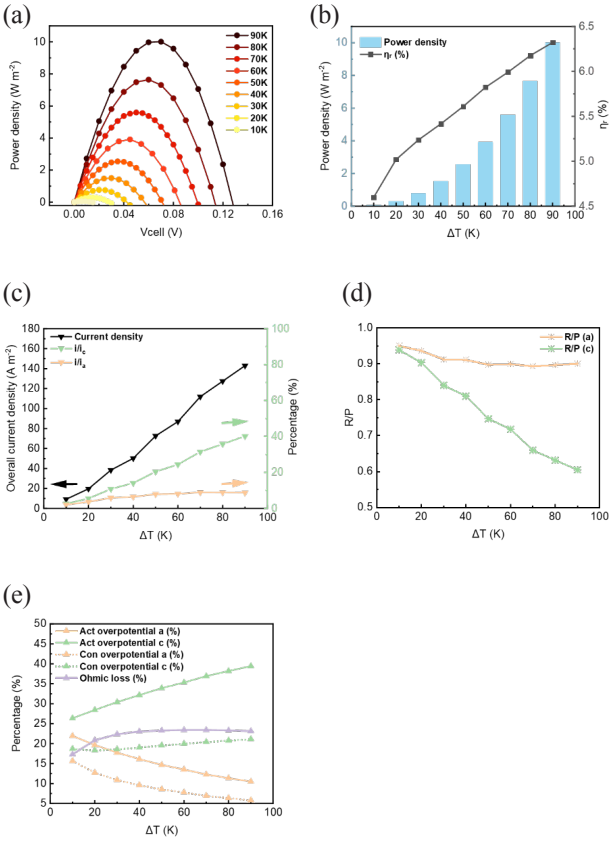

Figure 5. Effect of temperature difference. (a) The performances of power density versus increasing working voltage given various temperature differences. Square thermocell of 2.6 mm in length corresponding to the reported design with electrodes placed vertically. The anode and cathode are at the left- and right-hand side respectively; (b) the power densities and efficiencies; (c) current densities and their proportions to exchange current density; (d) the ratio of reactants to products of the anode and cathode; and (e) overpotential proportions to the overall overpotential under the working conditions of peak power.

3.5. Effect of thermocell arrangement and electrode surface

Since it has been proved that the power density is maximum when the length and width are equal (Salazar et al., 2014), a square shape was used to study the arrangement effect. In this analysis, the temperature difference, cell size and concentration were set to be 86 K, 2.6 mm and 0.9 M respectively. From Figure 6(a), it can be easily found that the power density is higher when the electrode is placed vertically than that when placed horizontally, which is consistent with the results in the literature (Qian et al., 2017). This is because the natural convection caused by the density difference greatly affects the mass transfer process on the cathode surface. From Figures 6(b) and 6(c), it can also be seen that when the electrodes are placed in different directions, the temperature gradient on the cathode surface obviously changes. When the electrodes are placed vertically, the temperature gradient on the surface of the cathode is larger, leading to a stronger convection. When a thermocell is limited by the electrode kinetics of the cathode, vertical placement is indeed better than horizontal placement. By fixing the electrode placement and the average electrode distance between the two electrodes as shown in Figures 6(d) and 6(e), the electrode is designed to have a ribbed structure with even spaces. The essence of this is to investigate the electrode area influence on current density and power density. As a result, the ribbed cathode works under a current density of 195.45 A m^{-2} and a power density of 11.727 W m^{-2}, which are slightly higher than those of the plate electrode (180.73 A m^{-2}, 10.844 W m^{-2}) and those of the ribbed anode (173.96 A m^{-2}, 10.437 W m^{-2}). The finding lends support to our assumption that the power density is hindered by the relatively slow kinetics of the cold electrode. Consequently, enlarging the cathode area (cold electrode) is more efficient than tuning the anode as an overly complex electrode surface conversely prevents the mass transfer of the anode. In addition to the abovementioned comparison of anode and cathode, an interesting phenomenon found in Figures 6(e) to 6(g) is the nonproportional relation of electrode surface area or mean distance from anode to cathode, which is concluded in Figure 6(h). The power densities in Figures 6(e) to 6(g) are predictably higher than that of the plate electrodes with a distance of 1.3 mm; however, the power densities stabilise at approximately 11.5 W m^{-2} rather than increase with the cathode area. When exclusively taking the cathode area into consideration, the results seem inconsistent with the hypothesis. This can be explained by the current distribution in Figures 6(e) to 6(g), from which the high current density occurs at the cathode surface closest to the

heat source and diminishes rapidly at the channel depth exceeding 1 mm due to low mass transfer. These findings allow the inference that, from the perspective of electrode design, a larger power density is dominated by the closest distance between the cathode and the anode as well as the area of cathode near this distance. A rational design of bilaterally ribbed electrode structure in Figure 6(i) satisfying the suggestions given above, exhibits an average power density of 13.462 W m^{-2} (per total area of electrode). If the mass transfer problem at the end corner of the cell can be solved by circulating the electrolyte, while the problem of easy short circuit in practical applications can be solved by the separator, this design is worth trying for the purpose of promoting power density. This value can even be further increased by replacing the solid cathode with a foam metal electrode or porous carbon electrode.

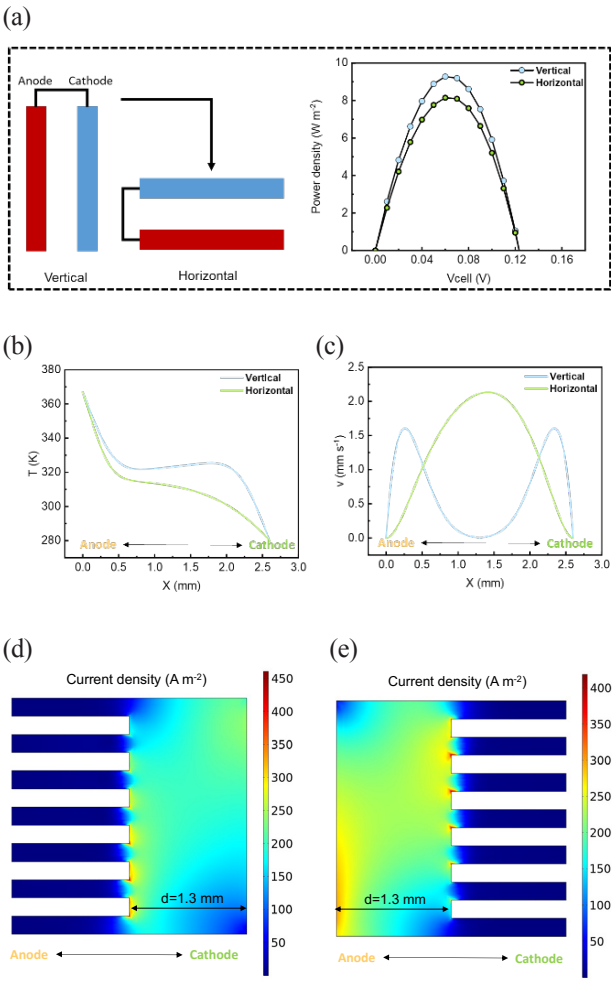

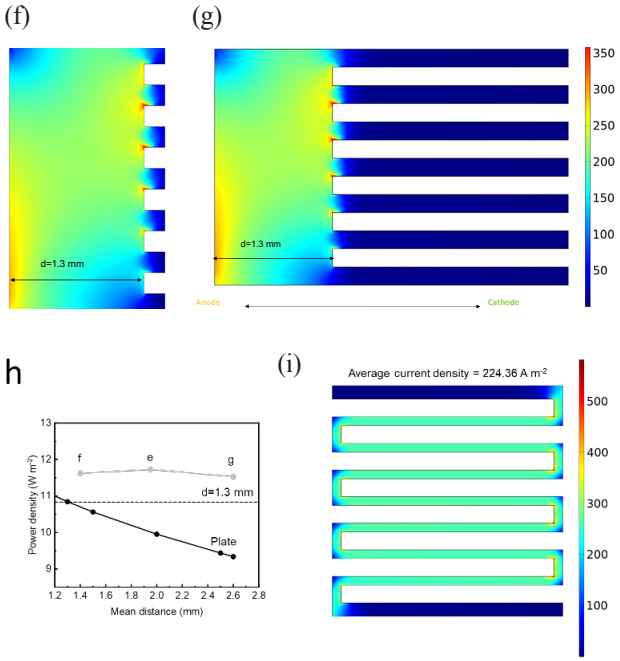

Figure 6. The comparison of the influence of electrode placement direction on power density. (a) The power density of vertical and horizontal placement of electrodes; (b) temperature distribution on the centre line perpendicular to the electrode direction; (c) velocity of the electrolyte in the cell; (d) the current density performance of thermocells with a rib configuration of anode (high temperature); and (e) cathode (low temperature). The distance between the ribbed electrode and the counted electrode is the same in these two cases of Figures 6(d) and 6(e). The current density performance of thermocells with different rib structures of cathode. Under the same distance between the anode and left end of the rib, the lengths of the rib are controlled as 0.2 mm (Figure 6(f)), 1.3 mm (Figure 6(e)) and 2.6 mm (Figure 6(g)). The power densities corresponding to Figures 6(e), 6(f) and 6(g) are plotted in Figure 6(h); and (i) The current density performance of a thermocell with a bilaterally ribbed electrode structure.

3.6. Effect of location and thickness of separator

The effect of separator placement and thickness on power density was also briefly studied. The parameters here are the same as when investigating the effect of thermocell arrangement and electrode surface. In order to ensure good mechanical properties under stable flowing liquid in practical applications, the thickness of the separator should not be too thin and should be less than the distance between the two electrodes. Thus, the thickness of the separator was set between 0.5 and 2 mm. The separator was set at the anode, the cathode and between the two electrodes respectively (Figure 7(a)). As shown in Figure 7(b), when the separator is placed in the middle and on the anode side, the power densities are about 10 W m^{-2} or below. When the separator is placed on the cathode side, the power density

can be increased by nearly 30% and can reach 12 W m^{-2}. According to the ratio of reactants and products on the cathode surface, the use of a separator on the cathode surface leads to more uniform species distribution on the cathode surface. This means that the use of a separator at the cathode side benefits the mass transfer process of the cathode. If the separator is regarded as a porous medium domain, the mass transfer process of ions is mainly controlled by convection and diffusion. As referred to above in the section on size investigation, strong convection can positively affect the mass transfer of the electrode surface, which is dominated by diffusion. In terms of this diffusion-convection process in pure aqueous electrolyte, the diffusion layer is usually very thin and becomes thinner as natural convection becomes stronger (Salazar et al., 2014). Therefore, although there is a temperature gradient in the diffusion layer, the diffusion coefficient can still be regarded as a constant. And a larger temperature difference near the electrode surface will result in power convection, further leading to higher power output. But for porous media, this process will be more complicated. The sponge is used as the separator material with a thermal conductivity of about 0.4 W m^{-1} K^{-1}, which is less than that of pure electrolyte (0.6 W m^{-1} K^{-1}). This further indicates that the temperature difference between the two sides of the separator is higher than that without the separator, so the convection is stronger. The existence of the separator reduces the cross-sectional area through which the fluid passes, and also increases the fluid flow rate. But a large temperature difference also leads to a lower average temperature inside the separator, which leads to a lower ion diffusion rate. In addition, a more important point is that the thickness of the diffusion layer and the influence of convection on the diffusion layer on the electrode surface must be carefully considered here. In this case, the thickness of the diffusion layer cannot be ignored. And how the process of convection and diffusion affect each other needs to be further studied. The reason why the thickness of the diffusion layer is important is that it is in inverse proportion to the limiting current density. When the thickness is very small, the influence of diffusion on the electrode reaction is not as great as the electrode reaction rate itself. However, when the thickness of the diffusion layer becomes larger, the limiting diffusion current density decreases sharply, and the electrochemical reaction becomes complicated. Additional experimental data is required to describe the process. These referred factors should be considered in a more complete model. Experiments will be conducted in future work. According to Figure 7(c), the total mass transfer intensity can still be inferred from the ratio of reactants to products at the cathode. A larger ratio means a more even species distribution caused by stronger mass transfer, which is beneficial to power output. It is certain that the presence of a separator does not necessarily reduce the power density.

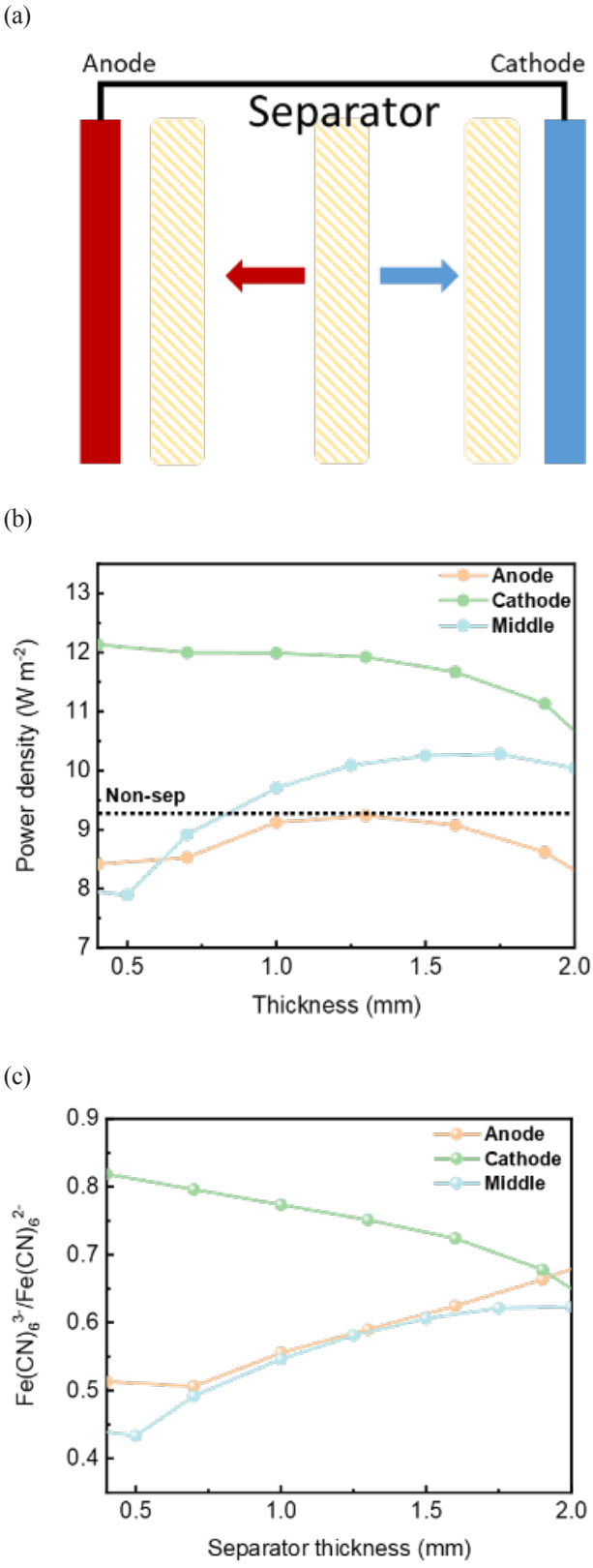

Figure 7. Effect of location and thickness of the separator. (a) Diagram of thermocells with a separator; (b) the performances of power density when the separator is set from the anode side to cathode side (0.9 M, ΔT=86 K); and (c) concentration proportion on the surface of the cathode in Figure 7(b).

4. Conclusion

This work investigates the effects of operational and structural parameters on the performance of thermocells using a mathematical model. It is found that the performance of thermocells is restricted by the slow electrochemical electrode kinetics and mass transfer process of the cold electrode (cathode in the present study). As the kinetics and mass transfer process are related to temperature and concentration, increasing the concentration of redox couple and widening the operating temperature window to enlarge the temperature difference of two electrodes are beneficial to the peak power density and efficiency. In a thermocell design, vertical placement of electrodes demonstrates a 13.85% higher power density than horizontal placement of electrodes. Appropriately increasing the area of the cathode closest to the anode, such as by using a porous electrode or designing the electrode morphology, helps enlarge the power density. Therefore, a rational design of a bilaterally ribbed electrode structure produces an average power density of 13.462 W m^{-2} (per total area of electrode). It is also found that the temperature distribution near the cathode greatly affects the cathode reaction. Applying a porous separator with lower thermal conductivity to enlarge the temperature gradient on the cathode surface could enhance the convective mass transfer process, thereby increasing the power density. It turns out that the power density is increased by approximately 30% if a separator with a relatively low thermal conductivity is attached to the cathode in comparison to the non-separator condition. For thermocells working at a high current density, increasing the concentration of redox couple helps to reduce the three types of overpotentials. The concentration overpotential can be reduced by increasing the convection intensity. The ohmic loss can be reduced by adding supporting electrolyte with high solubility and high charge. The further improvement of thermocells requires a redox couple with a higher temperature coefficient, electrolyte with lower thermal conductivity and higher conductivity, as well as electrodes with faster kinetics to maximise the power density and efficiency. They are the necessary requirements for the practical application of thermocells.

Acknowledgments

M Ni thanks the funding support from The Hong Kong Polytechnic University <P0014036> and a grant <PolyU 152064/18E> from Research Grant Council, University Grants Committee of Hong Kong. S P Feng thanks the funding support from Research Grants Council of Hong Kong under Award Numbers <17206519> and <17203520>.

Notes on contributors

Ms Chun Cheng is now a Ph.D. student of the Department of Building and Real Estate at The Hong Kong Polytechnic University. Her research background is in electrochemistry and chemical engineering. Now her research focuses on the electrochemical method of heat to electricity conversion.

Prof Shien Ping Feng is a Professor at the Department of Advanced Design and Systems Engineering (ADSE), City University of Hong Kong. He received his B.S., M.S. and Ph.D. from National Tsing Hua University. He was a postdoctoral associate at Massachusetts Institute of Technology and was working in the semiconductor industry before entering academia. His current research focuses on the development of electrochemical technology for energy harvesting and recycling. He is an elected Fellow of the Institute of Materials, Minerals and Mining and is the co-founder and founder of two start-up companies respectively.

Prof Meng Ni received his Ph.D. from The University of Hong Kong. Currently, he is a Professor and Associate Dean (Faculty of Construction and Environment) at The Hong Kong Polytechnic University. His research interests include fuel cells, rechargeable batteries and electrochemical systems for low-grade heat utilisation. Prof Ni is a Senior Editor for Sustainable Energy Technologies and Assessments (Elsevier) and an Associate Editor for two other journals. He is an active reviewer for over 80 academic journals.

References

[1] Cheng C, Dai Y, Yu J, Liu C, Wang S, Feng SP and Ni M (2020). Review of liquid based systems to recover low-grade waste heat for electrical energy generation. *Energy & Fuels*, pp. 161–175.

[2] Cui Y, Wang Y, Shao Z, Mao A, Gao W and Bai H (2020). Smart sponge for fast liquid absorption and thermal responsive self-squeezing. *Advanced Materials*, 32(14), 1908249.

[3] Daum PH and Enke CG (1969). Electrochemical kinetics of the ferri-ferrocyanide couple on platinum, *Analytical Chemistry*, 41(4), pp. 653–656.

[4] Hu R, Xu D and Luo X (2020). Liquid thermocells enable low-grade heat harvesting. *Matter*, 3(5), pp. 1400–1402.

[5] Ikeshoji T, Nahui FNB de, Kimura S and Yoneya M (1991). Computer analysis on natural convection in thin-layer thermocells with a soluble redox couple. *Journal of Electroanalytical Chemistry and Interfacial Electrochemistry*, 312(1–2), pp. 43–56.

[6] Kielland J (1937). Individual activity coefficients of ions in aqueous solutions, *Journal of the American Chemical Society*, 59(9). pp. 1675–1678.

[7] Kimura S (1991). Computer analysis of natural convection in thin-layer thermocells with a soluble redox couple Part 1. Method and the unsteady problem. *Journal of Electroanalytical Chemistry*, 307, pp. 29–45.

[8] Qian G, Lu Y, Huang Y, Li Z, Yu X and Roskilly AP (2017). Simulation study of Ferricyanide/Ferrocyanide concentric annulus thermocell with different electrode spacing and cell direction. *Energy Procedia*, 142, pp. 374–380.

[9] Qin Y, Zhang M and Mei G (2018). A new simplified method for measuring the permeability characteristics of highly porous media. *Journal of Hydrology*, 562, pp. 725–732.

[10] Quickenden TI and Mua Y (1995). A review of power generation in aqueous thermogalvanic cells. *Journal of The Electrochemical Society*, 142(11), pp. 3985–3994.

[11] Rahbar K, Mahmoud S, Al-Dadah RK, Moazami N and Mirhadizadeh SA (2017). Review of organic Rankine cycle for small-scale applications. *Energy Conversion and Management*, 134, pp. 135–155.

[12] Rahimi M, Straub AP, Zhang F, Zhu X, Elimelech M, Gorski CA and Logan BE (2018). Emerging electrochemical and membrane-based systems to convert low-grade heat to electricity. *Energy & Environmental Science*, 11(2), pp. 276–285.

[13] Salazar PF, Kumar S and Cola BA (2014). Design and optimization of thermo-electrochemical cells, *Journal of Applied Electrochemistry*, 12.

[14] Sarac H, Patrick MA, Wragg AA (1993). Physical properties of the ternary electrolyte potassium ferri-ferrocyanide in aqueous sodium hydroxide solution in the range 10-90°C. *Journal of Applied Electrochemistry*, 23, pp. 51-55.

[15] Sokirko AV (1994). Theoretical study of thermogalvanic cells in steady state. *Electrochimica Acta*, 39(4), pp. 597–609.

[16] Spiro M (1964a). Standard exchange current densities of redox systems at platinum electrodes. *Electrochimica Acta*, 9(11), pp. 1531–1537.

[17] Spiro M (1964b). Standard exchange current densities of redox systems at platinum electrodes. *Electrochimica Acta*, 9(11), pp. 1531–1537.

[18] Zhang L, Kim T, Li N, Kang TJ, Chen J, Pringle JM, Zhang M, Kazim AH, Fang S, Haines C, Al-Masri D, Cola BA, Razal JM, Di J, Beirne S, MacFarlane DR, Gonzalez-Martin A, Mathew S, Kim YH, Wallace G and Baughman RH (2017). High power density electrochemical thermocells for inexpensively harvesting low-grade thermal energy. *Advanced Materials*, 29(12), 1605652.